1521-009X/45/10/1093–1100$25.00
Drug Metabolism and Disposition

https://doi.org/10.1124/dmd.117.077081
Drug Metab Dispos 45:1093–1100, October 2017

Hepatocyte-Specific Deletion of EGFR in Mice Reduces Hepatic Abcg2 Transport Activity Measured by [^{11}C]erlotinib and Positron Emission Tomography

Alexander Traxl,[1] Karin Komposch,[1] Elisabeth Glitzner,[1] Thomas Wanek, Severin Mairinger, Oliver Langer,[2] and Maria Sibilia[2]

Center for Health and Bioresources, Biomedical Systems, AIT Austrian Institute of Technology GmbH, Seibersdorf, Austria (A.T., T.W., S.M., O.L.); Institute of Cancer Research, Department of Medicine I, Comprehensive Cancer Center (K.K., E.G., M.S.); Department of Clinical Pharmacology (O.L.) and Department of Biomedical Imaging and Image-Guided Therapy, Division of Nuclear Medicine (O.L.), Medical University of Vienna, Vienna, Austria

Received June 20, 2017; accepted August 4, 2017

ABSTRACT

The epidermal growth factor receptor (EGFR) regulates cellular expression levels of breast cancer resistance protein (humans: ABCG2, rodents: Abcg2) via its downstream signaling pathways. Drugs that inhibit EGFR signaling (e.g., tyrosine kinase inhibitors, antibodies) may lead to ABCG2-mediated drug-drug interactions (DDIs) by changing the disposition of concomitantly administered ABCG2 substrate drugs. In this study, we used positron emission tomography and magnetic resonance imaging to compare disposition of the model Abcg2 substrate [^{11}C]erlotinib in a mouse model of hepatocyte-specific deletion of EGFR (EGFR$^{\Delta hep}$ mice, n = 5) with EGFR$^{fl/fl}$ control mice (n = 6), which have normal EGFR expression levels in all tissues. Integration plot analysis was used to estimate the rate constants for transfer of radioactivity from the liver into bile (k_{bile}) and from the kidney into urine (k_{urine}). EGFR$^{\Delta hep}$ mice showed significantly lower radioactivity concentrations in the intestine (1.6-fold) and higher radioactivity concentrations in the urinary bladder (3.2-fold) compared with EGFR$^{fl/fl}$ mice. K_{bile} was significantly decreased (3.0-fold) in EGFR$^{\Delta hep}$ mice, whereas k_{urine} was by 2.2-fold increased. Western blot analysis of liver tissue confirmed deletion of EGFR and showed significant decreases in Abcg2 and increases in P-glycoprotein (Abcb1a/b) expression levels in EGFR$^{\Delta hep}$ versus EGFR$^{fl/fl}$ mice. Our data show that EGFR deletion in hepatocytes leads to a reduction in Abcg2-mediated hepatobiliary clearance of a probe substrate accompanied by a shift to renal excretion of the drug, which raises the possibility that EGFR-inhibiting drugs may cause ABCG2-mediated DDIs.

Introduction

The ATP-binding cassette (ABC) transporter breast cancer resistance protein (ABC subfamily G member 2, humans: ABCG2, rodents: Abcg2) influences drug disposition as it recognizes diverse drugs and drug metabolites as its substrates (e.g., rosuvastatin, sulfasalazine, mitoxantrone, topotecan, prazosin, dantrolene, ciprofloxacin, erlotinib, gefitinib) (Lee et al., 2015; Mao and Unadkat, 2015). ABCG2 is expressed in the canalicular (bile-facing) membrane of hepatocytes and in the brush-border membrane of kidney proximal tubule cells, where it promotes hepatobiliary and urinary excretion of drugs or drug metabolites. ABCG2 also limits oral absorption of drugs in the small intestine and restricts the distribution of drugs in the brain, often in concert with P-glycoprotein (ABC subfamily B member 1, humans: ABCB1, rodents: Abcb1a/b), in brain capillary endothelial cells forming the blood-brain barrier. Alterations in ABCG2 transport activity from genetic polymorphisms or drug-drug interactions (DDIs) may lead to changes in the disposition of ABCG2 substrates, which may affect drug safety and efficacy. So far, ABCG2-mediated DDIs have been mainly studied in the intestine (Kruijtzer et al., 2002; Allred et al., 2011; Kusuhara et al., 2012; Custodio et al., 2014), and considerably less information is available with respect to DDIs that lead to changes in the hepatobiliary excretion of drugs. This is most likely related to the fact that intestinal DDIs can be assessed by studying drug plasma pharmacokinetics, whereas hepatic ABCG2-mediated DDIs may lead only to changes in drug concentrations in the liver and intestine without pronounced changes in drug plasma pharmacokinetics. For a better understanding of tissue DDIs, noninvasive positron emission tomography (PET) imaging with radiolabeled drugs has been proposed as a useful tool (Kusuhara, 2013; Langer, 2016).

Apart from direct inhibition of ABCG2, certain drugs may interfere with regulatory pathways controlling transporter expression in tissue, which could also give rise to transporter-mediated DDIs. It has, for instance, been shown in vitro using different cell lines that the epidermal

This work was supported by the Austrian Science Fund (FWF) [Grants F3518-B20, F3513-B20] and by the Lower Austria Corporation for Research and Education (NFB) [Grants LS12-006, LS15-003].

[1]A.T., E.G., and K.K. contributed equally to this study.

[2]O.L. and M.S. had equal responsibility for this study.

https://doi.org/10.1124/dmd.117.077081.

ABBREVIATIONS: ABC, adenosine triphosphate-binding cassette; ABCB1, human ABC subfamily B member 1, also known as P-glycoprotein; Abcb1a/b, rodent ABC subfamily B member 1A and 1B, also known as P-glycoprotein; ABCG2, human ABC subfamily G member 2, also known as breast cancer resistance protein; Abcg2, rodent ABC subfamily G member 2, also known as breast cancer resistance protein; AUC, area under the curve; DDI, drug-drug interaction; EGFR, epidermal growth factor receptor; EGFR$^{\Delta hep}$, transgenic mice lacking EGFR in hepatocytes; EGFR$^{fl/fl}$, transgenic mice harboring a loxP-flanked EGFR allele; PET, positron emission tomography; TKI, tyrosine kinase inhibitor.

growth factor receptor (EGFR) regulates cellular ABCG2 expression levels via its downstream signaling pathways [i.e., phosphatidyl-inositol 3-kinase (PI3K)/Akt, mitogen-activated protein kinase (MAPK)] (Takada et al., 2005; Meyer zu Schwabedissen et al., 2006; Pick and Wiese, 2012; Porcelli et al., 2014) (Fig. 1). EGFR-targeting tyrosine kinase inhibitors (TKIs) (e.g., gefitinib, erlotinib, afatinib, osimertinib), which are frequently used in the clinic for cancer treatment, inhibit EGFR-signaling pathways and may therefore cause a reduction in tissue ABCG2 expression levels, which could affect disposition of concomitantly administered ABCG2-substrate drugs; however, in vivo data on EGFR-mediated regulation of tissue ABCG2 expression levels are scarce. A possible confounding factor in the study of the influence of EGFR inhibition on ABCG2-mediated drug disposition may be the fact that most TKIs also directly inhibit ABCG2 transport activity (Hegedüs et al., 2012; D'Cunha et al., 2016). Recently, transgenic mouse models with cell type–specific hepatic deletion of EGFR have been described (Natarajan et al., 2007; Lanaya et al., 2014). Such mouse models lend themselves to studying in vivo the regulation of ABCG2 by EGFR in a "nonpharmacological" approach. A previous PET study has shown that hepatobiliary excretion of [^{11}C]erlotinib is mediated in mice by Abcg2 (Traxl et al., 2015).

In the present study, we used [^{11}C]erlotinib as a model Abcg2 substrate and compared its hepatic disposition, using PET and magnetic resonance (MR) imaging, in EGFR$^{\Delta hep}$ mice, which specifically lack EGFR in hepatocytes, with EGFR$^{fl/fl}$ mice, which have normal EGFR expression in all tissues. We hypothesized that deletion of EGFR in hepatocytes will lead to reduced hepatobiliary excretion of [^{11}C]erlotinib as a result of the downregulation of hepatic Abcg2.

Materials and Methods

Chemicals and Drugs. Unless otherwise stated, all chemicals were obtained from Merck (Darmstadt, Germany) or Sigma-Aldrich (St. Louis, MO). All chemicals were used without further purification and were of at least analytic grade.

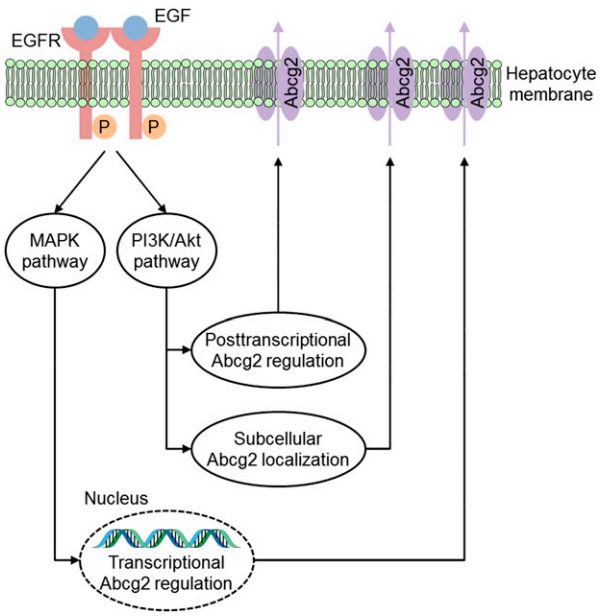

Fig. 1. Schematic illustration of a simplified model showing how the EGFR regulates cellular Abcg2 expression levels. After ligand binding, the EGFR tyrosine kinase activates several downstream signal transduction pathways, including the mitogen-activated protein kinase (MAPK) and the phosphatidyl-inositol 3-kinase (PI3K)/Akt pathway. It has been shown that EGF increases cellular Abcg2 expression via the MAPK pathway on both mRNA and protein levels (Meyer zu Schwabedissen et al., 2006). Furthermore, numerous studies suggested that EGF influences posttranscriptional regulation and subcellular localization of Abcg2 via the PI3K/Akt pathway (Mogi et al., 2003; Takada et al., 2005; Pick and Wiese, 2012; Porcelli et al., 2014).

Animals. Healthy male EGFR$^{\Delta hep}$ (lacking EGFR in hepatocytes of the liver, but not in other tissues) and EGFR$^{fl/fl}$ (harboring a loxP-flanked EGFR allele, having normal EGFR expression in all tissues) littermate control mice with a C57BL/6 background were generated as described previously (Natarajan et al., 2007) and bred in the mouse facilities of the Medical University of Vienna (Division of Decentralized Biomedical Research Facilities) according to federal guidelines and guidelines of the Medical University of Vienna (BMWFW-66.009/0199-WF/II/3b/2014). At the time of the experiment, animals weighed 22–33 g (EGFR$^{fl/fl}$: 31.2 ± 1.6 g, EGFR$^{\Delta hep}$: 25.7 ± 3.3 g) and were 13–15 weeks old. Animals were housed in individual ventilated polysulfon type III cages (five to six animals per cage) under controlled environmental conditions (24.0 ± 0.6°C, 40%–70% humidity, 12-hour light/dark cycle) with free access to tap water and standard rodent diet (Ssniff Spezialdiäten, Soest, Germany). An acclimatization period of at least 1 week was allowed before the animals were used in the experiments. All animal experiments were approved by the national authorities (Amt der Niederösterreichischen Landesregierung), and all study procedures were performed in accordance with the European Communities Council Directive of September 22, 2010 (2010/63/EU).

Radiotracer Synthesis. [^{11}C]Erlotinib was synthesized by *O*-[^{11}C]methylation of 6-*O*-desmethyl-erlotinib (OSI-420, Syncom BV, Groningen, The Netherlands) as described previously (Bahce et al., 2013). Specific activity at the time of injection was 74.8 ± 35.2 GBq/μmol (n = 11 batches), and radiochemical purity was >98%. For i.v. administration to animals, [^{11}C]erlotinib was formulated in 0.1 mM hydrochloric acid in physiologic saline at an approximate concentration of 555 MBq/ml.

PET/MR Imaging. EGFR$^{fl/fl}$ (n = 6) and EGFR$^{\Delta hep}$ (n = 5) mice each underwent an MR scan followed by a dynamic PET scan after i.v. injection of [^{11}C]erlotinib. For imaging, animals were preanesthetized in an induction chamber using isoflurane (Abbott Laboratories, Maidenhead, UK) and placed on a heated (37°C) animal bed, and the lateral tail vein was cannulated. Body temperature and respiration rate were constantly monitored (SA Instruments, Stony Brook, NY). Isoflurane anesthesia (1.5%–2.5% in oxygen) and heating were maintained for the entire imaging period. Anatomic whole-body MR imaging was performed on a 1-Tesla benchtop ICON scanner (Bruker, Ettlingen, Germany) using a modified T_1-weighted gradient echo sequence (T_1-fast low-angle shot) with the following parameters: echo time = 5 ms; repetition time = 25 ms; flip angle = 25°; field of view = 76 × 28 × 24 mm; matrix = 253 × 93; 32 slices; slice thickness = 0.75 mm; scan time = 6.25 minutes. For PET imaging, the animal bed was transferred into the gantry of a microPET Focus 220 system (Siemens Medical Solutions, Knoxville, TN), and a 10-minute transmission scan using a ^{57}Co point source was recorded. Subsequently, [^{11}C]erlotinib (46.9 ± 14.6 MBq, corresponding to 0.47 ± 0.54 μg (range: 0.07–2.05 μg) of unlabeled erlotinib, n = 11 batches) was administered as an i.v. bolus over 1 minute via the lateral tail vein, and a 90-minute dynamic PET scan was initiated at the start of radiotracer injection with an energy window of 250–750 keV and a timing window of 6 ns.

Postimaging Procedures. At the end of the PET scan, a terminal blood sample was withdrawn from the retro-orbital sinus vein, and the animals were sacrificed by cervical dislocation while still under deep anesthesia. The liver was removed, and the radioactivity of blood aliquots was measured in a Wallac Wizard 1470 γ-counter (PerkinElmer, Wellesley, MA). For protein extraction, total liver tissue was homogenized using a Precellys CK28 lysing kit (Bertin, Rockville, MD) containing the respective lysis buffer (for total cell extracts: RIPA buffer containing 50 mM Tris, pH 8.0, 150 mM sodium chloride, 1% Triton X-100, 0.5% sodium deoxycholate and 0.1% SDS; for membrane-enriched cell extracts: 50 mM HEPES, pH 7.3, 150 mM sodium chloride, 10% glycerol, 1% Triton X-100, 1 mM EDTA, and 1.5 mM magnesium chloride). The tissue was lysed using a Precellys Evolution Homogenizer (Bertin Instruments, Montigny-le-Bretonneux, France). Cell extracts were snap-frozen in liquid nitrogen and stored at −80°C until further processing.

Western Blotting. For Western blotting, frozen extracts were thawed and centrifuged at 12,000g at 4°C for 10 minutes. The protein concentration of the cleared lysate was determined using the Pierce BCA Protein Assay Kit (Thermo Fisher Scientific, Waltham, MA). Fifteen micrograms of lysed protein was resuspended in denaturing protein-loading buffer and left at room temperature for 10 minutes. Proteins were separated by SDS-PAGE and transferred to

polyvinylidene difluoride membranes. To determine EGFR, Abcg2, and Abcb1a/b protein expression levels, the following monoclonal rabbit antibodies were used in 1:1000 dilutions: EGFR (EGFR (D38B1) XP rabbit monoclonal antibody no. 4267), Abcg2 (ABCG2 (D5V2K) XP rabbit monoclonal antibody no. 42078), and Abcb1a/b (anti-P glycoprotein antibody [EPR10364-57] (ab170904)). α-Tubulin (monoclonal anti-α-tubulin antibody produced in mice) was used as the loading control in a 1:500 dilution. For analysis of protein expression levels in liver tissue, all obtained bands were quantified by densitometry using ImageJ software (National Institutes of Health, Bethesda, MD) and normalized to α-Tubulin.

PET Data Analysis. The dynamic PET data were sorted into 25 frames, which incrementally increased from 5 seconds to 20 minutes. All PET images were reconstructed using Fourier rebinning of the three-dimensional sinograms followed by a two-dimensional filtered back-projection with a ramp filter, resulting in a voxel size of 0.4 × 0.4 × 0.796 mm^3. The standard data correction protocol was applied to the dynamic PET data, including normalization, injection decay correction, and attenuation correction. By applying a calibration factor derived from imaging a cylindrical phantom with a known radioactivity concentration, PET units were converted into units of radioactivity. Using the medical image data examiner software AMIDE (Loening and Gambhir, 2003), the left ventricle of the heart (image-derived blood curve), liver, gallbladder, duodenum, intestine, left kidney, and urinary bladder were manually outlined on coregistered PET/MR images, and concentration-time curves expressed in units of percent of the injected dose per milliliter or per gram (%ID/mL or %ID/g) were derived. It was assumed that the sum of radioactivity in the gallbladder, the duodenum, and the intestine represented radioactivity in the bile excreted from the liver. From the concentration-time curves, the area under the curve (AUC) from 0 to 90 minutes was calculated using Prism 7 software (GraphPad Software, La Jolla, CA).

Integration Plot Analysis. To estimate the rate constants for transfer of radioactivity from blood into liver ($k_{uptake,liver}$, milliliters per minute per gram liver), from blood into kidney ($k_{uptake,kidney}$, milliliters per minute per gram kidney), from liver into bile (k_{bile}, min^{-1}), and from kidney into urine (k_{urine}, min^{-1}), a graphical analysis method (integration plot) was used as described previously (Shingaki et al., 2015; Traxl et al., 2015). $k_{uptake,liver}$ and $k_{uptake,kidney}$ were measured from 0.3 to 3.5 minutes after radiotracer injection using the integration plot method and eq. 1:

$$\frac{C_{t,organ}}{C_{t,blood}} = k_{uptake,organ} \times \frac{AUC_{0-t,blood}}{C_{t,blood}} + V_E, \quad (1)$$

where $C_{t,organ}$ is the radioactivity concentration in the liver or kidney at time t, and $C_{t,blood}$ is the radioactivity concentration in the left ventricle of the heart at time t. $AUC_{0–t,blood}$ represents the area under the concentration-time curve in the left ventricle of the heart from time 0 to time t. $K_{uptake,organ}$ can be obtained by performing linear regression analysis of a plot of $C_{t,organ}/C_{t,blood}$ versus $AUC_{0-t,blood}/C_{t,blood}$ and calculating the slope of the regression line. V_E is the y-intercept of the integration plot.

K_{bile} and k_{urine} were measured from 12.5 to 65 minutes after radiotracer injection using the integration plot method and eq. 2:

$$C_{t,organ} = k_{fluid} \times AUC_{0-t,organ} + V_E, \quad (2)$$

where $C_{t,organ}$ is the radioactivity concentration in the intestine (including the gallbladder and duodenum) or urinary bladder at time t. $AUC_{0–t,organ}$ represents the area under the concentration-time curve in the liver or kidney from time 0 to time t. K_{fluid} (k_{bile} or k_{urine}) can be obtained by performing linear regression analysis of a plot of $C_{t,organ}$ versus $AUC_{0–t,organ}$ and calculating the slope of the regression line. V_E is the y-intercept of the integration plot.

Statistical Analysis. All values are given as mean ± S.D. Statistical differences between groups were analyzed by two-tailed unpaired t tests using Prism 7 software. To assess correlations, the Pearson correlation coefficient (r) was calculated. The level of statistical significance was set to a P value of less than 0.05.

Results

[^{11}C]Erlotinib Disposition in EGFR$^{fl/fl}$ and EGFR$^{\Delta hep}$ Mice. We acquired [^{11}C]erlotinib PET/MR scans in EGFR$^{fl/fl}$ mice, which have normal EGFR expression in all tissues and in EGFR$^{\Delta hep}$ mice, in which EGFR was deleted in hepatocytes but not in other tissues. Representative coregistered coronal whole-body PET summation and MR images are shown in Fig. 2, indicating lower radioactivity content in the duodenum and intestine and higher radioactivity content in the urinary bladder of EGFR$^{\Delta hep}$ mice compared with EGFR$^{fl/fl}$ mice. In Figs. 3 and 4, concentration-time curves and AUCs of [^{11}C]erlotinib in blood, liver, and intestine are shown for both mouse models. Blood radioactivity concentrations were significantly, by 1.5-fold, higher in EGFR$^{\Delta hep}$ than in EGFR$^{fl/fl}$ mice (blood AUC, EGFR$^{fl/fl}$: 263±48 %ID/mL*min, EGFR$^{\Delta hep}$: 397±93 %ID/mL*min). Also, liver AUCs were significantly, by 1.4-fold, increased in EGFR$^{\Delta hep}$ compared with EGFR$^{fl/fl}$ mice, but liver-to-blood AUC ratios were not significantly different between the two mouse models (Table 1). Radioactivity concentrations in the intestine (including the gallbladder and duodenum) were significantly, by 1.6-fold, lower in EGFR$^{\Delta hep}$ mice (intestine AUC, EGFR$^{fl/fl}$: 1340±368 %ID/g*min, EGFR$^{\Delta hep}$: 866±86 %ID/g*min).

To quantitatively evaluate hepatic disposition of [^{11}C]erlotinib, we used a graphical analysis approach (integration plot analysis) using an image-derived blood curve to estimate the rate constants for transfer of radioactivity from blood into liver ($k_{uptake,liver}$) and from liver via bile into duodenum and intestine (k_{bile}). Radioactivity concentrations measured in the left ventricle of the heart in the last PET frame (70–90 minutes after radiotracer injection) showed a good correlation ($r = 0.735$, $P < 0.05$) with radioactivity concentrations measured with a γ-counter in the venous blood sample collected at the end of the PET scan (data not shown). In Fig. 5, integration plots and $k_{uptake,liver}$ and k_{bile} values are shown for both mouse models. $K_{uptake,liver}$ was not significantly different, whereas K_{bile} was significantly, by 3.0-fold, decreased in EGFR$^{\Delta hep}$ compared with EGFR$^{fl/fl}$ mice (Table 1).

We also studied the distribution of [^{11}C]erlotinib to the kidney and the urinary bladder and estimated the rate constants for transfer of radioactivity from blood into the kidney ($k_{uptake,kidney}$) and from the kidney into the urine (k_{urine}) (Fig. 6; Table 1). Radioactivity concentrations in the urinary bladder were significantly, by 3.2-fold, higher in EGFR$^{\Delta hep}$ mice (urinary bladder AUC, EGFR$^{fl/fl}$: 683±441 %ID/g*min, EGFR$^{\Delta hep}$: 2171±866 %ID/g*min). $K_{uptake,kidney}$ values did not differ between the two mouse models, whereas k_{urine} was significantly, by 2.2-fold, higher in EGFR$^{\Delta hep}$ mice.

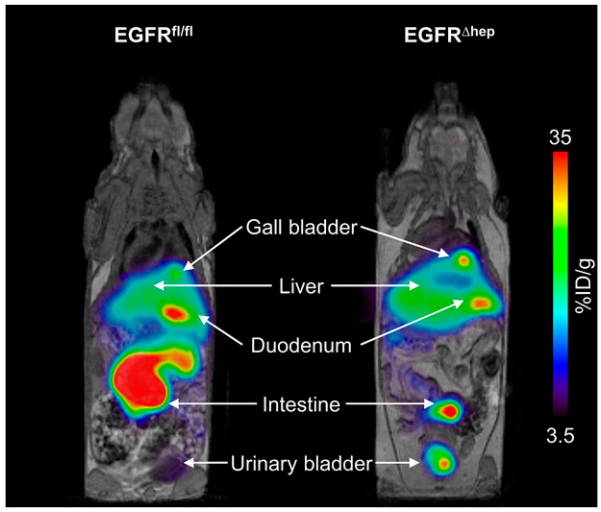

Fig. 2. Representative coregistered coronal whole-body [^{11}C]erlotinib PET summation (0–90 minutes) and MR (T_1-weighted gradient echo sequence) images of an EGFR$^{fl/fl}$ (left) and an EGFR$^{\Delta hep}$ (right) mouse. Anatomic structures are indicated by arrows. Radiation scale is set from 3.5% to 35% of the injected dose per gram (%ID/g) tissue.

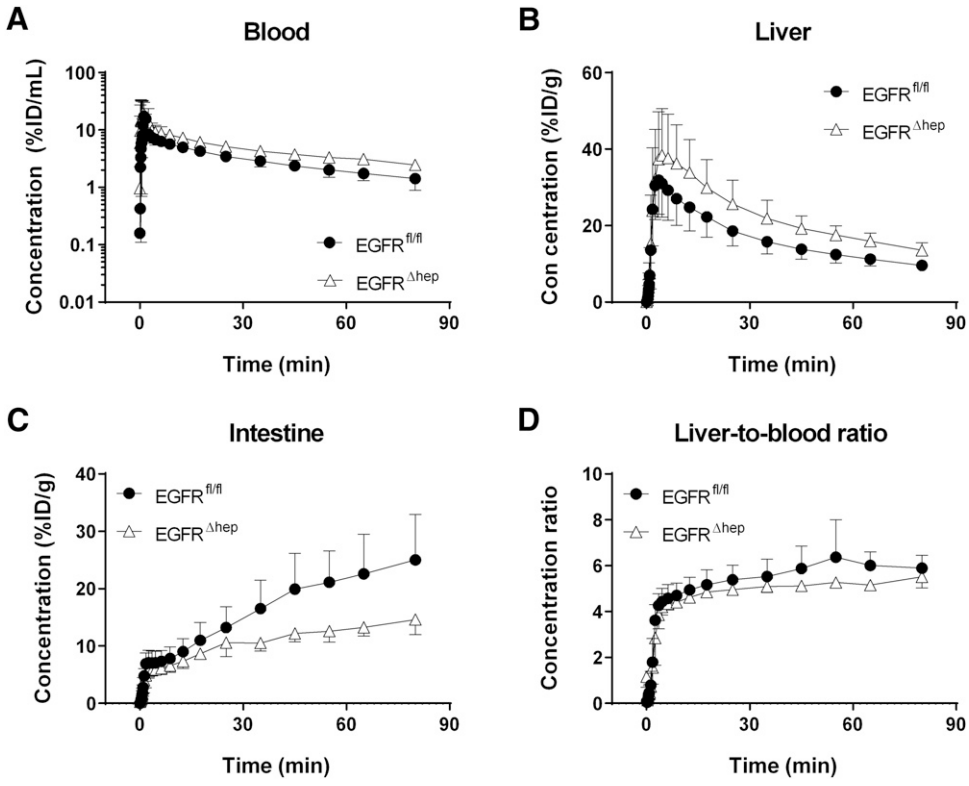

Fig. 3. Concentration-time curves (mean %ID/mL or %ID/g ± S.D.) of [^{11}C]erlotinib in blood (A), liver (B), and intestine (C), including gallbladder and duodenum) and liver-to-blood ratios (mean ± S.D.) over time (D) in EGFR$^{fl/fl}$ mice (filled circles, n = 6) and EGFR$^{\Delta hep}$ mice (open triangles, n = 5).

EGFR, Abcb1a/b, and Abcg2 Protein Expression Levels in Liver Tissue. Western blot analysis of liver tissue collected at the end of PET imaging confirmed an almost complete absence of EGFR protein expression levels in total cell extracts of EGFR$^{\Delta hep}$ mice compared with levels in EGFR$^{fl/fl}$ mice (on average 16.2-fold reduction, $P < 0.05$) (Fig. 7, A and B). The residual low EGFR signal in EGFR$^{\Delta hep}$ mice most likely derives from nonparenchymal cells, in which EGFR was not deleted. In EGFR$^{\Delta hep}$ mice, Abcg2 protein expression levels were significantly lower in total (on average, 2.9-fold), as well as in membrane-enriched (on average, 2.5-fold) cell extracts compared with EGFR$^{fl/fl}$ mice (Fig. 7, A and D), suggesting that the absence of EGFR does not affect the localization of the Abcg2 protein. In contrast, Abcb1a/b protein expression levels in the liver of EGFR$^{\Delta hep}$ mice were significantly increased in total cell extracts (on average, 3.1-fold), with a similar

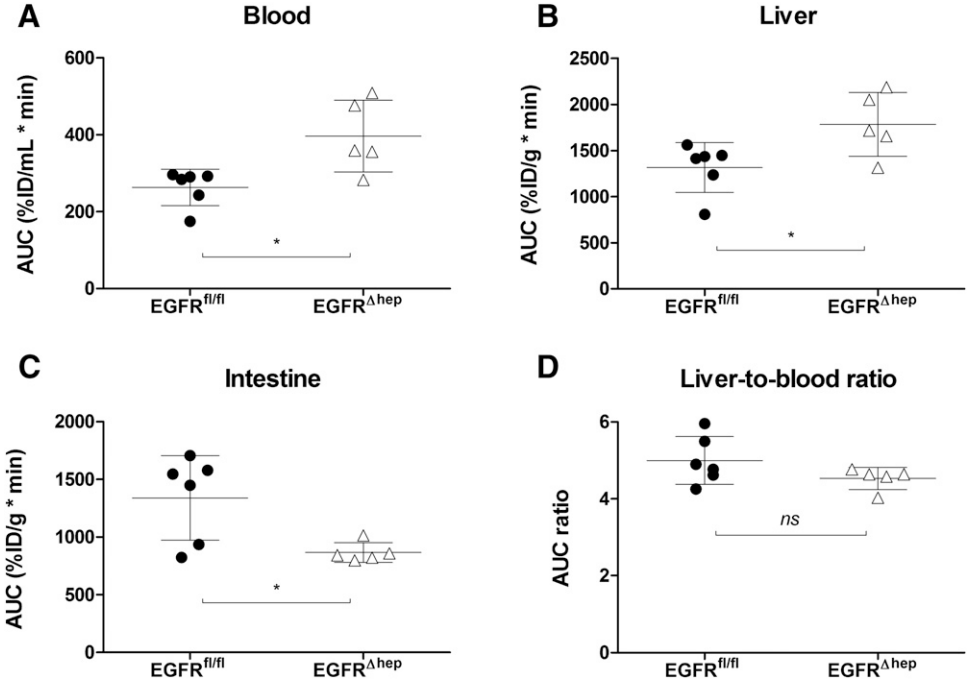

Fig. 4. Areas under the [^{11}C]erlotinib concentration-time curves (AUC, mean ± S.D.) for blood (A), liver (B) and intestine (C), including gallbladder and duodenum) and liver-to-blood (D) AUC ratios (mean ± S.D.) in EGFR$^{fl/fl}$ mice (filled circles, n = 6) and EGFR$^{\Delta hep}$ mice (open triangles, n = 5). ns, not significant, *$P < 0.05$, two-tailed unpaired t test.

TABLE 1

Pharmacokinetic parameters (mean ± S.D.) of [^{11}C]erlotinib in EGFR$^{fl/fl}$ mice (n = 6) and in EGFR$^{\Delta hep}$ mice (n = 5)

		AUC (min)	AUC ratio[a]	k_{uptake} (mL/min per g tissue)	k_{bile} (min^{-1})	k_{urine} (min^{-1})
Liver	EGFR$^{fl/fl}$	1315 ± 270	5.00 ± 0.62	0.799 ± 0.076	0.018 ± 0.003	—
	EGFR$^{\Delta hep}$	1783 ± 345*	4.53 ± 0.29	0.720 ± 0.151	0.006 ± 0.002***	—
Kidney	EGFR$^{fl/fl}$	677 ± 122	2.58 ± 0.26	0.458 ± 0.048	—	0.021 ± 0.015
	EGFR$^{\Delta hep}$	1197 ± 177***	3.07 ± 0.34*	0.434 ± 0.053	—	0.046 ± 0.013*

[a]Organ-to-blood AUC ratio.
*$P < 0.05$; ***$P < 0.001$ compared with EGFR$^{fl/fl}$ (two-tailed unpaired t test).

tendency in membrane-enriched cell extracts (on average, 2.3-fold) (Fig. 7, A and C).

Discussion

In this study, we compared the hepatic disposition of a microdose of the model Abcg2 substrate [^{11}C]erlotinib in EGFR$^{\Delta hep}$ and EGFR$^{fl/fl}$ mice to assess the EGFR-mediated regulation of hepatic Abcg2 transport activity. EGFR$^{\Delta hep}$ mice have a cell type-specific deletion of EGFR in hepatocytes, whereas EGFR$^{fl/fl}$ mice have normal EGFR expression levels in all tissues. EGFR$^{\Delta hep}$ mice are healthy and do not display any phenotypical abnormalities except for a reduction in body weight (Natarajan et al., 2007). As there is evidence for sex specific differences in EGFR pathways in the liver of mice (Wang et al., 2016) and as the assessment of these sex differences was not the subject of the present study, we focused on male mice in our experiments. Several previous studies have provided evidence for a regulatory link between EGFR signaling and ABCG2 expression (Fig. 1). It has been shown that the epidermal growth factor (EGF) can induce cell-surface expression of ABCG2 via the MAPK pathway (Meyer zu Schwabedissen et al., 2006). Moreover, the PI3K/Akt pathway, a downstream signal transduction pathway of EGFR, plays a crucial role in the posttranscriptional regulation of ABCG2 expression and its subcellular localization (Mogi et al., 2003; Takada et al., 2005; Pick and Wiese, 2012; Porcelli et al., 2014). For instance, treatment of ABCG2-overexpressing LLC-PKI cells with a PI3K inhibitor resulted in an internalization of ABCG2 from the apical surface and a decrease in the relative expression level of ABCG2 on the cell surface (Takada et al., 2005). These regulatory pathways may either be exploited, for instance, to overcome transporter-mediated chemoresistance of cancer cells, or they could also lead to unwanted DDIs, when a drug that interferes with EGFR signaling is combined with another drug that is transported by ABCG2. Most studies examining the regulation of ABC transporters have used cellular systems, and few in vivo data are available to assess whether modulation of regulatory pathways translates into alterations of transporter-mediated disposition of probe substrates (Slosky et al., 2013; Wang et al., 2014). Recent work has shown that PET with radiolabeled transporter substrates is a powerful tool to noninvasively measure the activities of different ABC and solute carrier transporters in the living organism (Kusuhara, 2013; Langer, 2016).

Erlotinib is a first-generation EGFR-targeting TKI and is approved for the treatment of non–small cell lung and pancreatic cancer. Erlotinib has also been suggested as potential treatment of hepatocellular carcinoma, although a recent phase 3 study was unable to demonstrate survival

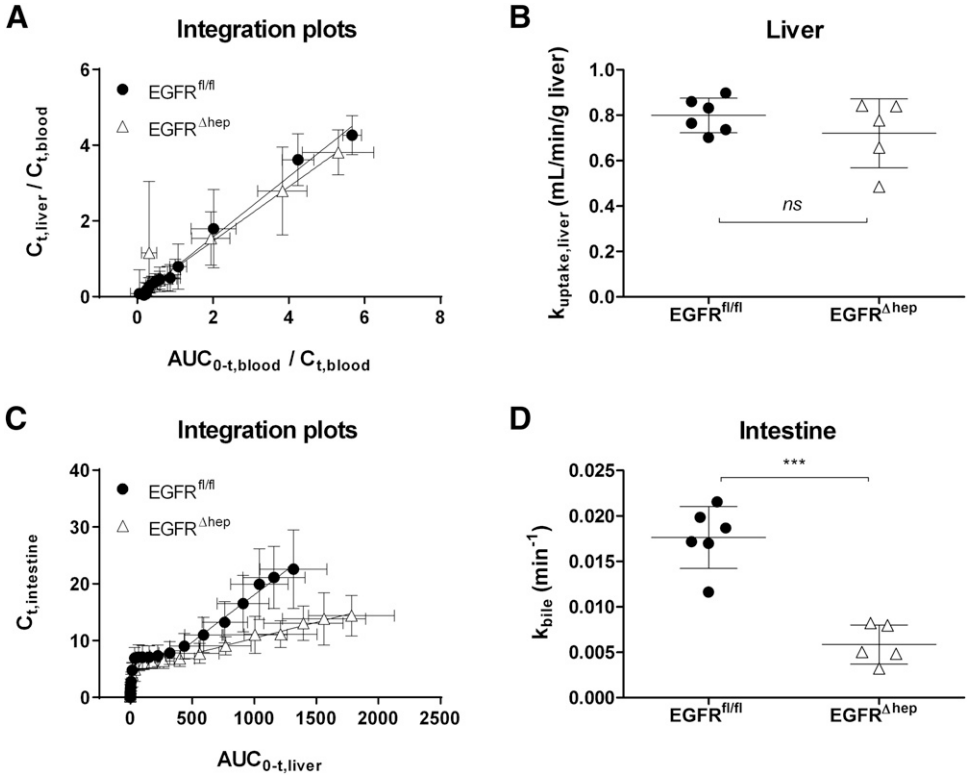

Fig. 5. Integration plots (mean ± S.D.) to estimate the rate constants for transfer of radioactivity from blood into liver ($k_{uptake,liver}$) (A and B) and from liver into bile (k_{bile}) (C and D) in EGFR$^{fl/fl}$ mice (filled circles, n = 6) and EGFR$^{\Delta hep}$ mice (open triangles, n = 5) mice. See *Materials and Methods* section for the definition of variables used in the integration plots. $K_{uptake,liver}$ and k_{bile} correspond to the slopes of the linear regression lines. ns, not significant, ***$P < 0.001$, two-tailed unpaired t test.

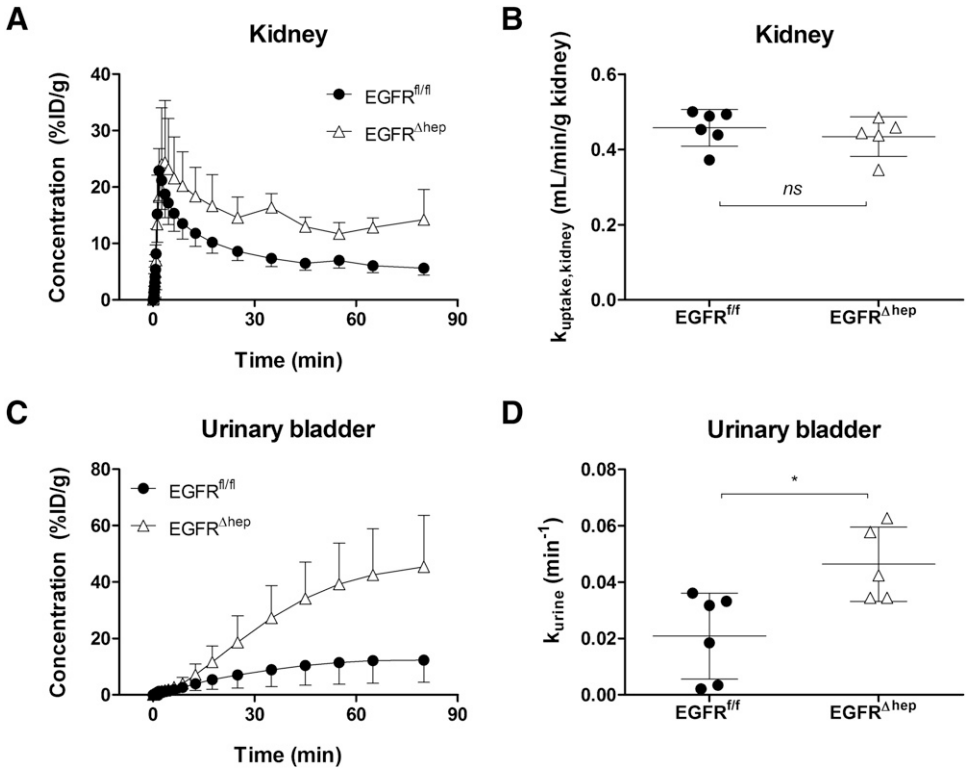

Fig. 6. Concentration-time curves (mean %ID/g ± S.D.) of [^{11}C]erlotinib in left kidney (A) and urinary bladder (C) and rate constants for transfer of radioactivity from blood into kidney ($k_{uptake,kidney}$) (B) and from kidney into urine (k_{kurine}) (D) in EGFR$^{fl/fl}$ mice (filled circles, $n = 6$) and EGFR$^{\Delta hep}$ mice (open triangles, $n = 5$). ns, not significant, $^*P < 0.05$, two-tailed unpaired t test.

improvement with erlotinib in advanced-stage HCC (Zhu et al., 2015). Erlotinib is excreted predominantly via the hepatobiliary route; in humans, 83% of an i.v. dose was excreted in feces and only 8% in urine (Ling et al., 2006). Erlotinib is a substrate of ABCG2 and ABCB1 (Kodaira et al., 2010) and has been shown to inhibit these transporters at higher concentrations (Shi et al., 2007). Moreover, there is evidence that erlotinib downregulates cellular ABCG2 expression levels via EGFR inhibition (Porcelli et al., 2014). We recently demonstrated

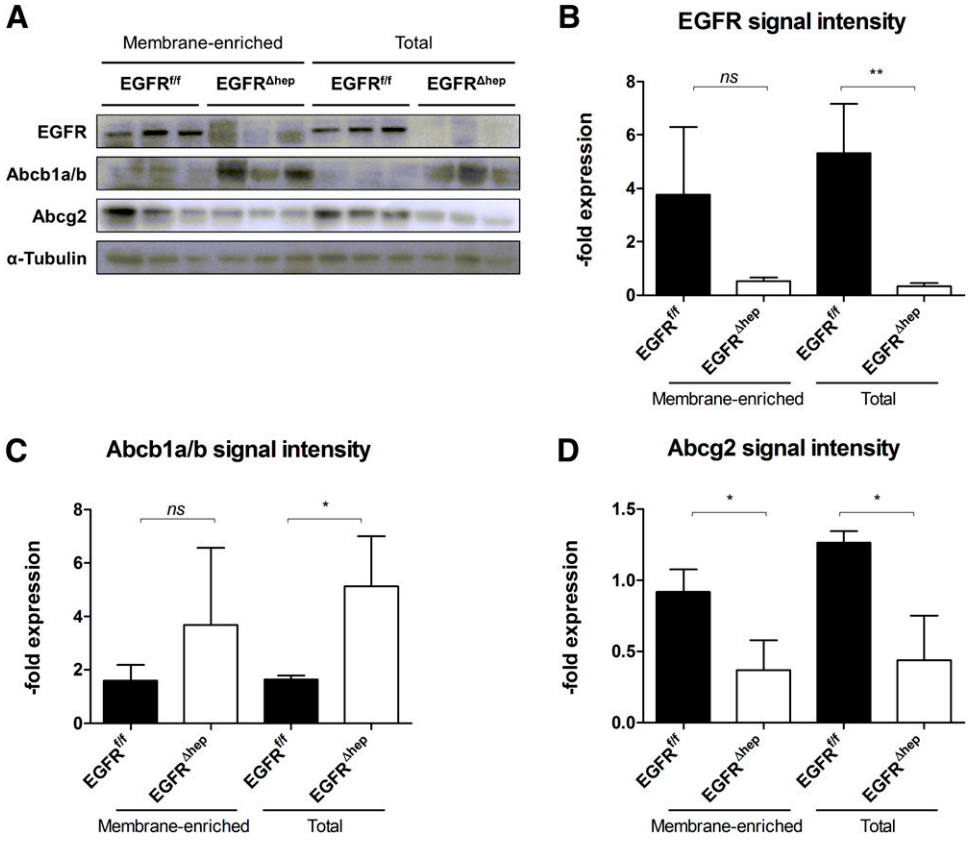

Fig. 7. Western blot analysis of EGFR, Abcb1a/b, and Abcg2 protein expression levels in liver tissue collected after the PET scan from EGFR$^{fl/fl}$ mice ($n = 3$) and EGFR$^{\Delta hep}$ mice ($n = 3$) using membrane-enriched and total cell extracts (A). Bands were quantified by densitometry using ImageJ software, and protein expression levels were normalized to α-tubulin, which was used as loading control (B–D). ns, not significant, $^*P < 0.05$, $^{**}P < 0.01$, two-tailed unpaired t test.

that k_{bile} of [^{11}C]erlotinib was 1.3-, 2.3-, and 2.8-fold reduced in Abcb1a/b$^{(-/-)}$, Abcg2$^{(-/-)}$, and Abcb1a/b$^{(-/-)}$Abcg2$^{(-/-)}$ mice, respectively, relative to wild-type mice (Traxl et al., 2015). Moreover, we found that most of the radioactivity in plasma, liver, and bile was composed of unmetabolized [^{11}C]erlotinib after i.v. injection of the radiotracer into wild-type mice, whereas only radiolabeled metabolites were detected in urine. These data provided evidence that hepatobiliary excretion of [^{11}C]erlotinib is mediated in mice by Abcg2 and, to a lesser extent, by Abcb1a/b, suggesting that [^{11}C]erlotinib may be used as a PET probe substrate to measure Abcg2 transport activity in the liver. In the present study, we used [^{11}C]erlotinib to investigate whether the deletion of EGFR in hepatocytes leads to changes in hepatic Abcg2 transport activity. To obtain quantitative pharmacokinetic parameters of hepatic disposition of [^{11}C]erlotinib, we estimated the transfer rate constants of radioactivity from blood into the liver ($k_{uptake,liver}$) and from the liver into bile (k_{bile}) using integration plot analysis (Shingaki et al., 2015; Traxl et al., 2015) (Fig. 5). K_{bile} is a parameter that has been used in other studies to assess canalicular ABC transport activities, such as that of Abcg2, in the liver of mice (Takashima et al., 2013).

$K_{uptake,liver}$ values were not significantly different in EGFR$^{\Delta hep}$ and EGFR$^{fl/fl}$ mice and ranged from 0.72 to 0.80 mL/min per gram of liver tissue, corresponding to a hepatic extraction ratio of 0.72–0.80 (assuming a hepatic blood flow rate in mice of approximately 1.0 mL/min per gram of liver tissue) (Davies and Morris, 1993) (Fig. 5B). $K_{uptake,liver}$ values in EGFR$^{fl/fl}$ mice were comparable to those measured in an earlier study in another mouse strain (FVB wild-type mice, $k_{uptake,liver}$: 0.734 $\pm$ 0.106 mL/min per gram of tissue), indicating good reproducibility of our analytical method (Traxl et al., 2015). There is evidence that hepatic uptake of [^{11}C]erlotinib is transporter-mediated, as reflected by a decrease in $k_{uptake,liver}$ in wild-type mice coinjected with a therapeutic dose of unlabeled erlotinib compared with mice that only received a PET microdose of [^{11}C]erlotinib (Traxl et al., 2015); however, in contrast to certain low-permeability drugs, for which hepatic disposition is to a large extent transporter-mediated (e.g., statins), erlotinib is a highly lipophilic compound that can be expected to also penetrate cellular membranes by passive diffusion. K_{bile} was 3.0-fold lower in EGFR$^{\Delta hep}$ mice (Fig. 5D), suggesting a decrease in the biliary excretion of [^{11}C]erlotinib. The decrease in total, as well as in membrane-bound, hepatic Abcg2 expression levels in EGFR$^{\Delta hep}$ mice as revealed by Western blot analysis (Fig. 7D) suggested transcriptional regulation of Abcg2 protein levels by EGFR rather than an alteration in the membrane localization of Abcg2. Interestingly, there was an increase in hepatic Abcb1a/b expression levels (Fig. 7C), which is in line with another study that assessed changes in transporter expression levels in human conditionally immortalized proximal tubule epithelial cells after treatment with the EGFR recombinant antibody cetuximab; significant decreases occurred in ABCG2 mRNA and increases were seen in ABCB1 mRNA (Caetano-Pinto et al., 2017). Our data thus support the premise that hepatobiliary excretion of [^{11}C]erlotinib is, to a larger extent, dependent on Abcg2 than on Abcb1a/b, as k_{bile} was decreased in EGFR$^{\Delta hep}$ mice despite an apparent upregulation of canalicular Abcb1a/b. Our data also provide evidence that [^{11}C]erlotinib PET is a sensitive tool to measure changes in Abcg2 transport activity in the liver.

Despite the decrease in radioactivity excreted into bile, liver profiles were parallel (Fig. 3B) and liver-to-blood AUC ratios were not significantly different in both mouse models, with a tendency for lower values in EGFR$^{\Delta hep}$ mice (Fig. 4D). On the other hand, blood AUC values were significantly higher in EGFR$^{\Delta hep}$ mice (Fig. 4A). This result could be related to an increase in the transfer of [^{11}C]erlotinib across the basolateral (sinusoidal) membrane from the liver into the blood in EGFR$^{\Delta hep}$ mice, possibly involving basolateral efflux transporter(s), as potential compensatory mechanism for the decrease in biliary excretion. However, this remains speculative as the rate constant for transfer of radioactivity from liver into blood could not be determined with the presently used analysis approach.

Because erlotinib partly undergoes urinary excretion (Ling et al., 2006), we also measured distribution of [^{11}C]erlotinib to the kidneys and urinary bladder (Fig. 6). In a previous study, we found that urinary excretion of radioactivity after i.v. injection of [^{11}C]erlotinib was quite low in wild-type mice and markedly increased in Abcg2$^{(-/-)}$ and Abcb1a/b$^{(-/-)}$Abcg2$^{(-/-)}$ mice (Traxl et al., 2015), suggesting a shift from hepatobiliary to renal excretion (which was apparently not mediated by renal Abcg2 and Abcb1a/b), when hepatobiliary excretion was impaired owing to knockout of Abcg2. A similar phenomenon was observed in the present study, in which k_{urine} was 2.2-fold higher in EGFR$^{\Delta hep}$ compared with EGFR$^{fl/fl}$ mice (Fig. 6D).

Our in vivo data confirm previous in vitro data showing that EGFR signaling can regulate ABCG2 expression levels (Mogi et al., 2003; Takada et al., 2005; Meyer zu Schwabedissen et al., 2006; Pick and Wiese, 2012; Porcelli et al., 2014). We provide, to our knowledge, the first evidence that EGFR deletion in hepatocytes translates in vivo into a decrease in Abcg2 transport activity leading to changes in the disposition of an Abcg2 probe substrate. Our findings may have clinical relevance as they raise the possibility that treatment with EGFR inhibitors, such as TKIs or antibodies, may alter hepatic ABCG2 transport activity and thereby lead to changes in hepatobiliary clearance of concomitantly administered ABCG2 substrate drugs, which potentially could lead to hepatotoxicity of drugs but also could prove beneficial in the treatment of liver tumors by prolonging the residence times of anticancer drugs in the liver, if their biliary excretion is dependent on ABCG2 transport activity. It should be noted that our study was conducted with a microdose of erlotinib (~120-fold lower than a human oral therapeutic dose of 2 mg/kg). As erlotinib itself is a potent inhibitor of ABCG2 (IC_{50}: 0.13 μM) (Noguchi et al., 2009), ABCG2 transport activity may be saturated in the liver at therapeutic erlotinib doses, which may result in less pronounced effects of EGFR deletion on the disposition of a therapeutic dose of erlotinib. Transgenic mouse models with cell type-specific deletion of regulatory pathways or transporters may serve as valuable tools to assess the impact of transporters on drug disposition.

Acknowledgments

We thank Johann Stanek, Thomas Filip, Michael Sauberer, and Mathilde Löbsch (AIT Austrian Institute of Technology GmbH) for performing the PET/MR imaging experiments.

Authorship Contributions

Participated in research design: Komposch, Wanek, Langer, Sibilia.

Conducted experiments: Traxl, Komposch, Glitzner, Wanek, Mairinger.

Performed data analysis: Traxl, Komposch, Glitzner, Wanek, Mairinger, Langer.

Wrote or contributed to the writing of the manuscript: Traxl, Komposch, Glitzner, Wanek, Mairinger, Langer, Sibilia.

References

Allred AJ, Bowen CJ, Park JW, Peng B, Williams DD, Wire MB, and Lee E (2011) Eltrombopag increases plasma rosuvastatin exposure in healthy volunteers. *Br J Clin Pharmacol* **72**:321–329.

Bahce I, Smit EF, Lubberink M, van der Veldt AA, Yaqub M, Windhorst AD, Schuit RC, Thunnissen E, Heideman DA, Postmus PE, et al. (2013) Development of [(^{11})C]erlotinib positron emission tomography for in vivo evaluation of EGF receptor mutational status. *Clin Cancer Res* **19**:183–193.

Caetano-Pinto P, Jamalpoor A, Ham J, Goumenou A, Mommersteeg M, Pijnenburg D, Ruijtenbeek R, Sanchez-Romero N, van Zelst B, Heil SG, et al. (2017) Cetuximab prevents methotrexate-induced cytotoxicity in vitro through epidermal growth factor dependent regulation of renal drug transporters. *Mol Pharm* **14**:2147–2157.

Custodio JM, Wang H, Hao J, Lepist EI, Ray AS, Andrews J, Ling KH, Cheng A, Kearney BP, and Ramanathan S (2014) Pharmacokinetics of cobicistat boosted-elvitegravir administered in combination with rosuvastatin. *J Clin Pharmacol* **54**:649–656.

Davies B and Morris T (1993) Physiological parameters in laboratory animals and humans. *Pharm Res* **10**:1093–1095.
D'Cunha R, Bae S, Murry DJ, and An G (2016) TKI combination therapy: strategy to enhance dasatinib uptake by inhibiting Pgp- and BCRP-mediated efflux. *Biopharm Drug Dispos* **37**: 397–408.
Hegedüs C, Truta-Feles K, Antalffy G, Várady G, Német K, Özvegy-Laczka C, Kéri G, Őrfi L, Szakács G, Settleman J, et al. (2012) Interaction of the EGFR inhibitors gefitinib, vandetanib, pelitinib and neratinib with the ABCG2 multidrug transporter: implications for the emergence and reversal of cancer drug resistance. *Biochem Pharmacol* **84**:260–267.
Kodaira H, Kusuhara H, Ushiki J, Fuse E, and Sugiyama Y (2010) Kinetic analysis of the cooperation of P-glycoprotein (P-gp/Abcb1) and breast cancer resistance protein (Bcrp/Abcg2) in limiting the brain and testis penetration of erlotinib, flavopiridol, and mitoxantrone. *J Pharmacol Exp Ther* **333**:788–796.
Kruijtzer CM, Beijnen JH, Rosing H, ten Bokkel Huinink WW, Schot M, Jewell RC, Paul EM, and Schellens JH (2002) Increased oral bioavailability of topotecan in combination with the breast cancer resistance protein and P-glycoprotein inhibitor GF120918. *J Clin Oncol* **20**: 2943–2950.
Kusuhara H (2013) Imaging in the study of membrane transporters. *Clin Pharmacol Ther* **94**: 33–36.
Kusuhara H, Furuie H, Inano A, Sunagawa A, Yamada S, Wu C, Fukizawa S, Morimoto N, Ieiri I, Morishita M, et al. (2012) Pharmacokinetic interaction study of sulphasalazine in healthy subjects and the impact of curcumin as an in vivo inhibitor of BCRP. *Br J Pharmacol* **166**: 1793–1803.
Lanaya H, Natarajan A, Komposch K, Li L, Amberg N, Chen L, Wculek SK, Hammer M, Zenz R, Peck-Radosavljevic M, et al. (2014) EGFR has a tumour-promoting role in liver macrophages during hepatocellular carcinoma formation. *Nat Cell Biol* **16**:972–977.
Langer O (2016) Use of PET imaging to evaluate transporter-mediated drug-drug interactions. *J Clin Pharmacol* **56** (**Suppl 7**):S143–S156.
Lee CA, O'Connor MA, Ritchie TK, Galetin A, Cook JA, Ragueneau-Majlessi I, Ellens H, Feng B, Taub ME, Paine MF, et al. (2015) Breast cancer resistance protein (ABCG2) in clinical pharmacokinetics and drug interactions: practical recommendations for clinical victim and perpetrator drug-drug interaction study design. *Drug Metab Dispos* **43**:490–509.
Ling J, Johnson KA, Miao Z, Rakhit A, Pantze MP, Hamilton M, Lum BL, and Prakash C (2006) Metabolism and excretion of erlotinib, a small molecule inhibitor of epidermal growth factor receptor tyrosine kinase, in healthy male volunteers. *Drug Metab Dispos* **34**:420–426.
Loening AM and Gambhir SS (2003) AMIDE: a free software tool for multimodality medical image analysis. *Mol Imaging* **2**:131–137.
Mao Q and Unadkat JD (2015) Role of the breast cancer resistance protein (BCRP/ABCG2) in drug transport–an update. *AAPS J* **17**:65–82.
Meyer zu Schwabedissen HE, Grube M, Dreisbach A, Jedlitschky G, Meissner K, Linnemann K, Fusch C, Ritter CA, Völker U, and Kroemer HK (2006) Epidermal growth factor-mediated activation of the map kinase cascade results in altered expression and function of ABCG2 (BCRP). *Drug Metab Dispos* **34**:524–533.
Mogi M, Yang J, Lambert JF, Colvin GA, Shiojima I, Skurk C, Summer R, Fine A, Quesenberry PJ, and Walsh K (2003) Akt signaling regulates side population cell phenotype via Bcrp1 translocation. *J Biol Chem* **278**:39068–39075.
Natarajan A, Wagner B, and Sibilia M (2007) The EGF receptor is required for efficient liver regeneration. *Proc Natl Acad Sci USA* **104**:17081–17086.
Noguchi K, Kawahara H, Kaji A, Katayama K, Mitsuhashi J, and Sugimoto Y (2009) Substrate-dependent bidirectional modulation of P-glycoprotein-mediated drug resistance by erlotinib. *Cancer Sci* **100**:1701–1707.
Pick A and Wiese M (2012) Tyrosine kinase inhibitors influence ABCG2 expression in EGFR-positive MDCK BCRP cells via the PI3K/Akt signaling pathway. *ChemMedChem* **7**:650–662.
Porcelli L, Giovannetti E, Assaraf YG, Jansen G, Scheffer GL, Kathman I, Azzariti A, Paradiso A, and Peters GJ (2014) The EGFR pathway regulates BCRP expression in NSCLC cells: role of erlotinib. *Curr Drug Targets* **15**:1322–1330.
Shi Z, Peng XX, Kim IW, Shukla S, Si QS, Robey RW, Bates SE, Shen T, Ashby CR Jr, Fu LW, et al. (2007) Erlotinib (Tarceva, OSI-774) antagonizes ATP-binding cassette subfamily B member 1 and ATP-binding cassette subfamily G member 2-mediated drug resistance. *Cancer Res* **67**:11012–11020.
Shingaki T, Hume WE, Takashima T, Katayama Y, Okauchi T, Hayashinaka E, Wada Y, Cui Y, Kusuhara H, Sugiyama Y, et al. (2015) Quantitative evaluation of mMate1 function based on minimally invasive measurement of tissue concentration using PET with [^{11}C]metformin in mouse. *Pharm Res* **32**:2538–2547.
Slosky LM, Thompson BJ, Sanchez-Covarrubias L, Zhang Y, Laracuente ML, Vanderah TW, Ronaldson PT, and Davis TP (2013) Acetaminophen modulates P-glycoprotein functional expression at the blood-brain barrier by a constitutive androstane receptor-dependent mechanism. *Mol Pharmacol* **84**:774–786.
Takada T, Suzuki H, Gotoh Y, and Sugiyama Y (2005) Regulation of the cell surface expression of human BCRP/ABCG2 by the phosphorylation state of Akt in polarized cells. *Drug Metab Dispos* **33**:905–909.
Takashima T, Wu C, Takashima-Hirano M, Katayama Y, Wada Y, Suzuki M, Kusuhara H, Sugiyama Y, and Watanabe Y (2013) Evaluation of breast cancer resistance protein function in hepatobiliary and renal excretion using PET with ^{11}C-SC-62807. *J Nucl Med* **54**:267–276.
Traxl A, Wanek T, Mairinger S, Stanek J, Filip T, Sauberer M, Müller M, Kuntner C, and Langer O (2015) Breast cancer resistance protein and P-glycoprotein influence in vivo disposition of ^{11}C-erlotinib. *J Nucl Med* **56**:1930–1936.
Wang L, Xiao J, Gu W, and Chen H (2016) Sex difference of Egfr expression and molecular pathway in the liver: impact on drug design and cancer treatments? *J Cancer* **7**:671–680.
Wang X, Campos CR, Peart JC, Smith LK, Boni JL, Cannon RE, and Miller DS (2014) Nrf2 upregulates ATP binding cassette transporter expression and activity at the blood-brain and blood-spinal cord barriers. *J Neurosci* **34**:8585–8593.
Zhu AX, Rosmorduc O, Evans TR, Ross PJ, Santoro A, Carrilho FJ, Bruix J, Qin S, Thuluvath PJ, Llovet JM, et al. (2015) SEARCH: a phase III, randomized, double-blind, placebo-controlled trial of sorafenib plus erlotinib in patients with advanced hepatocellular carcinoma. *J Clin Oncol* **33**:559–566.

Address correspondence to: Oliver Langer, Center for Health and Bioresources, Biomedical Systems, AIT Austrian Institute of Technology GmbH, 2444 Seibersdorf, Austria. E-mail: oliver.langer@ait.ac.at; or Maria Sibilia, Institute of Cancer Research, Department of Medicine I, Comprehensive Cancer Center, Medical University of Vienna, Borschkegasse 8a, A-1090 Vienna, Austria. E-mail: maria.sibilia@meduniwien.ac.at